Large Eddy Simulation of Atmospheric Convective Boundary Layer with Realistic Environmental Forcings

Aaron M. Botnick and Evgeni Fedorovich

School of Meteorology, University of Oklahoma, Norman, OK 73019, USA
botnicam@ou.edu, fedorovich@ou.edu

Abstract. Initializing large eddy simulations (LES) in meteorological applications typically involves prescribing an idealized background atmospheric environment in which simulations are run. This study investigates LES initialization options using realistic atmospheric environmental forcings. Analysis of several simulated convective boundary layer (CBL) cases highlights common sources of initialization-related errors in LES predictions of CBL structure and evolution as compared to observational data. Effects of initialization errors on simulated features of the CBL for different evolution patterns of daytime environmental atmospheric flow are analyzed. Possible approaches toward dynamic adjustment of environmental parameters in LES of atmospheric boundary layer flows are suggested.

Keywords: Large eddy simulation, Initialization, Convective boundary layer, Atmospheric observations, Meteorological radar profiler

1 Introduction

Turbulent flow structure in the clear convective boundary layer (CBL), which is commonly observed in the lower atmosphere during daytime hours, is primarily determined by buoyant heat transfer from the underlying surface. In conjunction with (wind) shear forcing, whose strength can be variable, this driving mechanism generates turbulent motions on a broad range of scales. This leads to a progressive deepening of the boundary layer as long as the surface buoyant forcing remains strong. The CBL typically develops in the stably stratified ambient atmosphere. Stratification strength is usually expressed in terms of the vertical gradient in the background potential temperature profile. This stratification can be weak (sometimes, almost neutral) – in this case, the CBL grows relatively fast. When stratification is strong, it effectively suppresses CBL growth into the free atmosphere aloft impeding entrainment of quiescent free-atmosphere air into the turbulent CBL core. Previous studies have shown that the surface buoyancy flux (combination of temperature

J. Meyers et al. (eds.), Quality and Reliability of Large-Eddy Simulations,

and moisture surface fluxes) in conjunction with the background atmospheric stratification and wind shear are the principal forcing mechanisms in the atmospheric CBL [10, 8, 12, 14, 2, 3]. Parameters of the ambient atmosphere in LES CBL studies conducted so far were typically prescribed in an idealized form, see e.g. [6]. In these applications, LES was used as a tool to evaluate, qualitatively and quantitatively, various physical mechanisms that determine CBL flow structure (in this respect, LES did a great job) rather than predicting particular features of the CBL flow structure under specific environmental conditions. Exceptions, in this sense, were studies by [12], who initialized their LES of sheared CBL with wind and potential temperature profile data from the U.S. Southern Great Plains (SGP) Atmospheric Radiation Measurement Climate Research Facility (ACRF), and by [4], who used observational data from different platforms during one day of the International H_2O Project (IHOP) field campaign in summer of 2002 to initialize LES of CBL in the vicinity of dryline. These two studies provided valuable, although limited (number of cases studied), information about the abilities of LES to handle real CBL flows coupled with the changing ambient atmosphere.

There is growing demand from the atmospheric remote-sensing community for high-resolution data on turbulence structure in atmospheric boundary layer flows to be used in radar and other remote-sensor simulators (see e.g. [13]). The CBL, where the dominant portion of turbulence energy is carried by large eddies with scales on the order of boundary layer depth, appears to be a natural subject for application of an LES-based turbulence data generator. However, in order to provide data for remote-sensor simulators operating under diverse weather conditions in the CBL, the LES should be able to adequately reproduce CBL turbulence dynamics with actual external forcings.

In the present study, LES runs have been conducted with realistic environmental atmospheric settings corresponding to particular summer days of 2004 and 2007 with clear CBLs observed at the SGP site. Besides providing data for evaluation of a radar simulator, the purpose of these numerical experiments was to evaluate accuracy of LES predictions with respect to various CBL features and investigate possible improvements of the LES settings to make the numerical predictions more accurate. After brief description of the employed LES code in Sect. 2, initialization procedures will be considered in Sect. 3, followed by a presentation of the analyzed LES data in conjunction with atmospheric soundings and radar observations in Sect. 4. Potential improvements of the LES setup will be addressed in Sect. 5.

2 Large Eddy Simulation

The LES code in use for this study employs the subgrid closure from [5]. Detailed explanation of the code can be found in [7], with revised boundary conditions described in [6]. Table 1 presents general LES settings employed. The time step for the LES runs was calculated from stability constraints,

Table 1 Settings of LES

Parameter	Setting
Domain size	5.12 x 5.12 x 4.0 km^3
Grid	256 x 256 x 200
Surface fluxes	See Eq. (9)
Geostrophic wind	Derived from RUC data as in Eq. (10)
Time step	Based on stability conditions: $\sim$ 0.6–1.2 s
Lateral BCs	Periodic for all variables
Upper BCs	Neumann with sponge layer in the upper 20% of domain
Lower BCs	No-slip for velocity; Neumann for θ, q, E (subgrid energy); Monin-Obukhov similarity functions as in [7]
Subgrid closure	Deardorff closure scheme as in [5]

varying between 0.4 and 1.2 s. Flow statistics were calculated every 50 time steps using horizontal averaging. Calculated statistics included means, variances, co-variances, and third-order moments. Simulations were initiated with vertical profiles of u (along x axis) and v (along y axis) components of the wind velocity, potential temperature (θ), specific humidity (q), x and y components of the geostrophic wind (u_g, v_g), and time series of fluxes of temperature ($\overline{w'\theta'}$) and moisture ($\overline{w'q'}$) measured at the underlying surface. The geostrophic wind represents the external forcing related to the horizontal gradient of the large-scale pressure field. Initialization procedure details are presented in Sect. 3. The governing equations for the employed LES are the following:

$$\frac{\partial \widetilde{u}_i}{\partial t} = -\frac{\partial \widetilde{u}_i \widetilde{u}_j}{\partial x_j} + g\frac{\widetilde{\theta}_v - \theta_{v_0}}{\theta_{v_0}}\delta_{i3} - \frac{\partial \widetilde{\pi}}{\partial x_i} + f\left(\widetilde{u}_j - u_{g_j}\right)\varepsilon_{ij3} + \frac{\partial}{\partial x_j}\left[\nu\left(\frac{\partial \widetilde{u}_i}{\partial x_j} + \frac{\partial \widetilde{u}_j}{\partial x_i}\right) - \left(\widetilde{u_i u_j} - \widetilde{u}_i\widetilde{u}_j\right)\right], \tag{1}$$

$$\frac{\partial \widetilde{u}_i}{\partial x_i} = 0\,, \tag{2}$$

$$\frac{\partial \widetilde{\theta}_v}{\partial t} = -\frac{\partial \widetilde{u}_i \widetilde{\theta}_v}{\partial x_i} + \frac{\partial}{\partial x_i}\left[\mu\left(\frac{\partial \widetilde{\theta}_v}{\partial x_i}\right) - \left(\widetilde{\theta_v u_i} - \widetilde{\theta}_v\widetilde{u}_i\right)\right], \tag{3}$$

where $i, j = \{1, 2, 3\}$; t is time, $x_i = (x, y, z)$ are the right-hand Cartesian coordinates, $\widetilde{u}_i = (\widetilde{u}, \widetilde{v}, \widetilde{w})$ represent resolved velocity components, $\widetilde{\theta}_v$ is resolved virtual potential temperature, ν is kinematic viscosity, and μ is molecular thermal diffusivity. Components of subgrid stresses and subgrid θ_v flux, respectively, are represented by $\widetilde{u_i u_j} - \widetilde{u}_i\widetilde{u}_j$ and $\widetilde{\theta_v u_i} - \widetilde{\theta}_v\widetilde{u}_i$. Tildes in these equations represent volume averaging. Normalized pressure, $\widetilde{\pi}$, is defined as $\widetilde{\pi} = \left(\widetilde{p} - p_0\right)/\varrho_0$, where $\widetilde{p}$ is resolved pressure, p_0 is hydrostatic atmospheric

pressure, ϱ_0 is constant reference density, and θ_{v_c} is constant reference potential temperature.

Subgrid stress and θ_v flux are parameterized in terms of subgrid eddy viscosity (K_m) and subgrid eddy diffusivity (K_h) following [5]:

$$\widetilde{u_i u_j} - \widetilde{u}_i \widetilde{u}_j = \frac{2}{3} E \delta_{ij} - 2K_m \widetilde{s_{ij}} \ , \tag{4}$$

$$\widetilde{\theta_v u_i} - \widetilde{\theta}_v \widetilde{u}_i = -K_h \frac{\partial \widetilde{\theta}_v}{\partial x_i} \ , \tag{5}$$

where $\widetilde{s_{ij}} = \left(\partial \widetilde{u}_i / \partial x_j + \partial \widetilde{u}_j / \partial x_i\right)/2$ is the deformation tensor for filtered velocity and E is subgrid kinetic energy, which is determined from the following balance equation:

$$\frac{\partial E}{\partial t} + \frac{\partial \widetilde{u}_i E}{\partial x_i} = 2K_m \widetilde{s_{ij}} \frac{\partial \widetilde{u}_i}{\partial x_j} - K_h \frac{\partial \widetilde{\theta}_v}{\partial x_3} + \frac{\partial}{\partial x_i}\left[2K_m \frac{\partial E}{\partial x_i}\right] - \varepsilon \ , \tag{6}$$

where ε represents the subgrid viscous dissipation rate. Eddy viscosity and diffusivity are expressed through mixing length l and E as

$$K_m = 0.12 l E^{1/2} \ , \ K_h = (1 + 2l/\Delta) K_m \ , \tag{7}$$

where $\Delta = (\Delta x \Delta y \Delta z)^{1/3}$ is effective grid-cell size, and $\varepsilon \propto \left(E^{3/2}/l\right)$.
Subgrid mixing length l is evaluated as

$$\begin{aligned} l &= \Delta \qquad \text{if } \partial \widetilde{b}/\partial z \le 0 \ , \\ l &= \min\left\{\Delta \ , \ 0.5E^{1/2} / \left(\partial \widetilde{b}/\partial z\right)^{1/2}\right\} \qquad \text{if } \partial \widetilde{b}/\partial z > 0 \ . \end{aligned} \tag{8}$$

A Poisson equation for $\widetilde{\pi}$ is constructed by combining the continuity and momentum balance equations as in [11]. This equation is solved numerically by the fast Fourier-transform technique over horizontal planes, and by tridiagonal matrix decomposition in the vertical.

3 Initialization Procedures

An example of typical initialization of LES with idealized atmospheric profiles is illustrated in panel (a) of Fig. 1; note that $u = u_g$ are held constant during the run as is $\overline{w'\theta'_v}$, with θ represented by a steady linear profile. In this study, LES is initialized with realistic environmental profiles schematically shown in panel (b) of Fig. 1. These realistic environmental settings often include multiple inversions (areas of higher stability) and sharp wind changes with height (wind shears). Under realistic conditions, $\overline{w'\theta'_v}$ at the surface is not

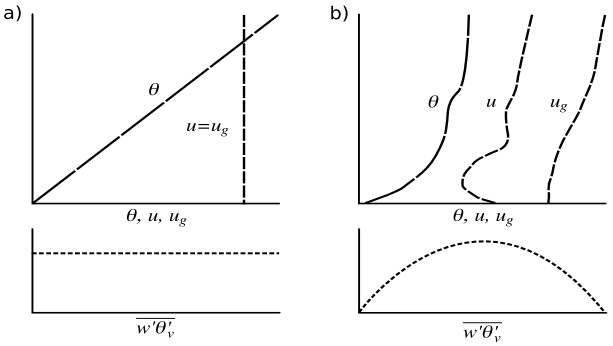

Fig. 1 Schematic representation of idealized (**a**) and realistic (**b**) initial data

taken constant, rather it reflects the evolution of the intensity of solar heating over the course of the day.

Initialization data for this study were collected from the SGP ACRF site in Lamont (north central Oklahoma) equipped with balloon borne instruments and an eddy-correlation system for measurement of surface fluxes. In our LES exercise, only clear CBLs were simulated, narrowing the number of possible cases. Surface fluxes of temperature and moisture were calculated from measured sensible and latent heat fluxes as

$$\overline{w'\theta'} = \frac{H}{\varrho_c\, c_p}\,, \qquad \overline{w'q'} = \frac{LH}{\varrho_c\, L_v}\,, \qquad \overline{w'\theta'_v} = \overline{w'\theta'} + 0.61\theta_{v_0}\overline{w'q'}\,, \quad (9)$$

In the above expressions, $\overline{w'\theta'}$ is surface kinematic temperature flux, $\overline{w'q'}$ is surface kinematic humidity flux, H is sensible heat flux, LH is latent heat flux (heat release from the condensation of water vapor), c_p is specific heat of water, and L_v is latent heat of vaporization. Geostrophic wind components are evaluated from the Rapid Update Cycle (RUC) [1] objective analysis system, these data are available hourly. Geostrophic wind is assumed the same in all vertical nodes of the LES domain. Four RUC grid points surrounding the Lamont (LMN) site are used in calculating horizontal gradients of pressure, deriving the geostrophic wind components as

$$u_g = \frac{-1}{\varrho_c f}\frac{\partial p}{\partial y}\,, \qquad v_g = \frac{1}{\varrho_c f}\frac{\partial p}{\partial x}\,, \qquad f = 2\Omega\sin\phi\,, \quad (10)$$

where f is the Coriolis parameter, Ω is the Earth's angular velocity, and ϕ is the site latitude. Profiles of actual wind, obtained either from RUC and/or from the local sounding at LMN, are interpolated to the vertical nodes of the LES domain. Near-surface portions of these profiles are additionally adjusted in order to match the no-slip condition at the surface, assuming the logarithmic wind profile throughout the lowest LES cell layer.

Two initialization methods were used in this study: local and composite. The local method uses data from the LMN site to obtain initial vertical profiles of θ, q, u, and v, while RUC analyses are used to calculate profiles of u_g and v_g. These profiles are specified only at model initialization time, and are not updated during the run. Surface fluxes, on the other hand, are updated every 30 min. Sounding data for LMN are available every 6 h, with 12 Coordinated Universal Time (UTC) (7 h local time) sounding data used for initialization. The LMN sounding data contain more than ten times that of traditional soundings from U.S. National Weather Service (NWS) sites. This allows more features of vertical atmospheric heterogeneity to be represented in the initial profiles. In contrast, composite initialization uses sounding data from five NWS sites as well as reduced resolution data from LMN aggregated into a single profile via an inverse distance weighted average. This procedure can be used for initialization of LES in locations where local data are not available. Initialized LES is then run for approximately 12 h of simulated time, or until the temperature flux becomes negative (sunset).

4 Case Description and Analysis

In central Oklahoma, only a few summer days normally contain a clear CBL throughout the course of the day. In order to identify clear CBL days, atmospheric radiation data from LMN were used. When no clouds are present, the diurnal distribution of solar radiation flux is represented by a smooth, nearly symmetric curve. As the employed LES uses temporally constant u_g and v_g to account for large-scale pressure forcing, an additional selection criterion was small variability of geostrophic wind throughout the 12 h period of simulation. This condition turned out to be rather restrictive (see discussion below).

The rationale for using atmospheric initialization with realistic environmental settings is to attempt accurate verification of LES statistics via remote-sensing platforms, such as meteorological profiling radars. Meaningful verification is possible if the LES is capable of reproducing a variety of remotely sensed features of the CBL: wind shears (both speed and directional), gradients of temperature and humidity, and capping inversion structure. The elevation, and especially the vertical extent, of the capping inversion are difficult to determine with any precision even in LES. In this study the maximum gradient of θ was used as an indicator of capping inversion height; taken, in turn, as a measure of CBL depth [15].

Pino et al. (2003) [12] attempted similar use of realistic atmospheric settings. However, their initial profiles were low resolution and remained semi-idealized. Their study, nevertheless, suggested that initializing LES with realistic settings was possible. The initial profiles of atmospheric variables in our study matched real atmospheric soundings as closely as possible. We also aimed at closely reproducing the observed sounding after 6 and 12 h of simulation. These times roughly corresponded to midday and sunset.

Prediction accuracy of CBL depth was used as a major criterion for quality of the LES in our application. We labeled a case fair when CBL depth was estimated within a few hundred meters of CBL depth from 0 UTC sounding data (12 h), and winds were in the same direction and close magnitude to those in 0 UTC sounding data. Cases were rated poor if after 12 h, CBL depth was off by a large margin or winds were vastly different from observational data.

4.1 Fair Case – 8 June 2007

Results shown for this case were obtained via the local initialization method, using RUC analyses on a higher-resolution grid (compared to 2004 cases). The considered case represented a unique atmospheric state. During the preceding night, a cold front had passed through LMN, where approximately 1.5 mm of rain fell. At 12 UTC, the upper atmosphere is still in transition between the trough associated with the cold front and the high pressure behind it. The LMN site is under an area of surface high pressure and light winds. Geostrophic wind components are -15 ms^{-1} (u_g) and -5 ms^{-1} (v_g) near the ground, as shown in Fig. 2. Both components considerably (and nearly synchronously) change in the vertical toward the domain top. Twelve h later (0 UTC) the geostrophic wind weakens to near zero as the vast area of high pressure moves further into the central plains.

The vertical wind distribution at 12 UTC displays a low-level jet (LLJ) with the peak wind speed at a height of about 700 m. Near-surface wind shear associated with this jet enhances vertical mixing early in the day. Eventually, as the CBL grows, the LLJ is completely mixed out, and the actual wind distribution becomes close to geostrophic. This can be seen in Fig. 3, where the LES profiles are shown at three times. Atmospheric stratification, according

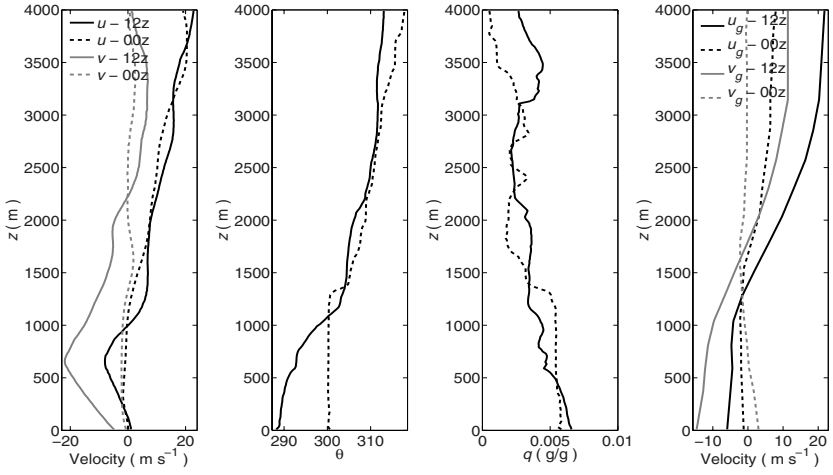

Fig. 2 Initial (12 UTC, *solid lines*) and observed (0 UTC, *dashed lines*) profiles

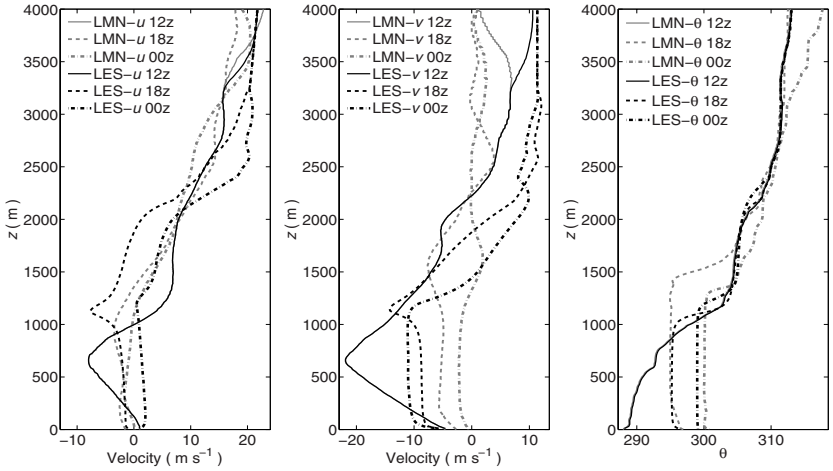

Fig. 3 LES (*black*) and LMN (*gray*) profiles at 12, 18, and 0 UTC for 8 June 2007

to the initial sounding is rather weak throughout the lower 500 m becoming stronger between 800 and 1200 m. This feature causes relatively fast growth of the CBL during the morning hours, with slower growth later in the day. Lamont sounding data at 0 UTC show CBL depth to be about 1300 m, with depth peaking near 1500 m at 18 UTC. A possible explanation for this CBL contraction is the movement of cooler air into the region behind the front that is not captured by the current version of the LES code. However, the CBL evolution predicted by LES for this case decently match the observed temporal changes of CBL depth with time over the main portion of the day. The procedures outlined in Sect. 5, in particular, temporal adjustment of geostrophic wind during the run and accounting for temperature advection, could further improve LES performance under atmospheric conditions similar to those observed in this case.

Meteorological radar profilers are able to detect vertical variability of the CBL structure, as they are sensitive to changes in the refractive index. This index may be directly expressed through air temperature and pressure, and additionally through water vapor mass concentration (specific humidity, q) for humid air. In the refractivity field, the CBL top is clearly seen as the boundary between warm, dry air in the free atmosphere aloft and cooler, moist air inside the CBL. Spatial variability of refractivity is represented by its structure function, C_n^2, defined in [13]. This quantity allows direct calculation from LES data. Radar range-corrected power, η, is related to C_n^2 as $\eta = 0.379 C_n^2 \lambda^{-1/3}$, where λ is the radar wavelength in cm. The LES-derived C_n^2 values for the considered CBL case in this section are compared in Fig. 4 (top panel) with C_n^2 derived from radar profiler measurements at the LMN site for this day. One can see that LES produces C_n^2 fields that closely match the trend in radar

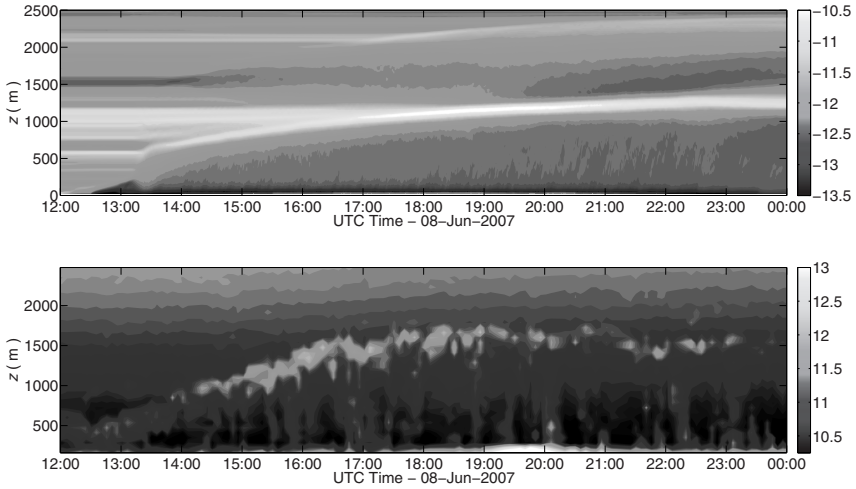

Fig. 4 LES-derived C_n^2 (*top*) and uncalibrated radar-derived C_n^2 (*bottom*)

data. Large values of C_n^2 in both plots show large fluctuations of temperatures and humidity near the CBL top.

4.2 Poor Case – 20 July 2004

Conditions at LMN on 20 July 2004 were characterized by high pressure with an approaching surface low and pre-frontal trough. No rainfall was reported, and winds were light with a 12 ms^{-1} LLJ present. There was minimal warming leading to a slight increase in the background θ profile, and slight changes in the background q profile. Geostrophic wind was almost constant in time in the x direction; however, significant changes took place, over the course of the day, in the y direction, as shown in Fig. 5. It is important to note that the initial θ profile in the considered case is nearly neutral, corresponding to very weak stratification. As a result, by the end of the day, the CBL depth is effectively undefined via sounding data, as mixing of CBL air with weakly stratified environmental air produces a deep CBL with poorly identifiable capping inversion (region with large θ gradient). Overall, the LES well captures this strong mixing and fast growth of the CBL, but it is almost impossible to derive any measurable integral parameters of the CBL (e.g. CBL and entrainment zone depth) for practical applications, see Fig. 6. Although the x component of the actual wind (u) is predicted quite accurately, the y component (v) is off by 8 ms^{-1} and points to the strong over-mixing of the corresponding component of momentum in this case.

Composite profile data were not available for initialization of this case, so it is hard to say whether they would produce better results given the initial background atmospheric state and its evolution over the course of the

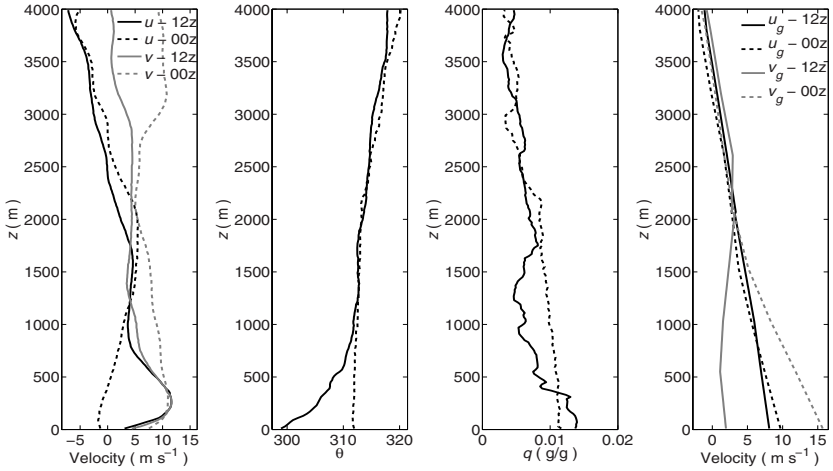

Fig. 5 Initial (12 UTC, *solid lines*) and observed (0 UTC, *dashed lines*) profiles

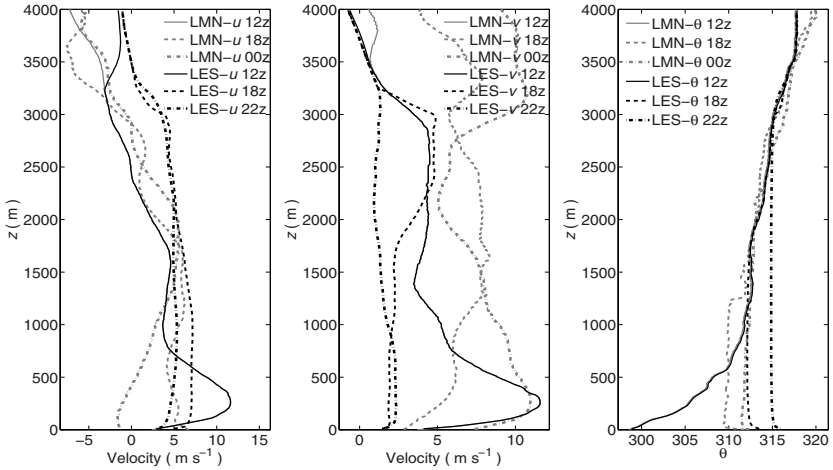

Fig. 6 LES (*black*) and LMN (*gray*) profiles at 12, 18, and 0 UTC for 20 July 2004

day. Apparently, any LES improvements are rather problematic in this case as many of the features that determine the CBL evolution under considered conditions are beyond current capabilities of LES designed for atmospheric boundary layer applications. To adequately account for these features, the LES should either be run in a nested mode with a larger-scale atmospheric model – such option has recently been discussed in [9] – or be fed with data from fine-scale, multi-platform atmospheric observations presently not readily available.

5 Potential Improvements of LES

Eight atmospheric CBL cases were analyzed in the reported LES exercise with the initialization procedures specified in Sect. 3. The performed analyses suggest that certain changes to the LES code may improve the prognostic capability of LES in a realistic atmospheric mode. These changes could include update of geostrophic wind profiles, adjustment of the background θ and q profiles in the process of CBL development, increasing temporal resolution of surface fluxes, and accounting for large-scale temperature advection (thermal wind).

While cases with weak winds and small temporal changes are reproduced well by LES, the majority of simulated cases showed some disparity between output statistics and observational data. With RUC analysis data available hourly, these data can be used to modify u_g and v_g profiles in the LES during the run resulting in a temporally changing geostrophic wind forcing. Availability of surface flux data with 5 min resolution (six time finer than currently employed) would help to more accurately adjust CBL evolution to the primary forcing driving this boundary layer flow.

The employed LES code does not take into account temperature advection associated with baroclinicity (thermal wind). In the context of the present LES exercise, the magnitude of the thermal wind is proportional to the vertical change in geostrophic wind, which can be retrieved from RUC analysis data. Incorporation of temperature advection in the LES equations would allow the θ profile to adjust to this large-scale forcing mechanism. A method for doing this can be found in [14], where LES was applied to simulate baroclinic mixed layers with idealized environmental atmospheric forcings. Generally, advection resulting in the evolution of initial profiles is very likely in the real atmosphere. It would be possible to account for such effects by gradualy adjusting the profiles of θ and q above the CBL, if information about their evolution were available.

Acknowledgements

The authors of this work wish to acknowledge the National Science Foundation (NSF) for their support via grant ATM-0553345. Observational data for this study were obtained from the Atmospheric Radiation Measurement (ARM) Program sponsored by the U.S. Department of Energy, Office of Science, Office of Biological and Environmental Research, Environmental Sciences Division.

References

1. Benjamin SG, Dévényi D, Weygandt SS, Brundage KJ, Brown JM, Grell GA, Kim D, Schwartz BE, Smirnova TG, Smith TL, Manikin GS (2004) An hourly assimilation-forecast cycle: the RUC. Mon Wea Rev 132:495–518

2. Conzemius RJ, Fedorovich E (2006) Dynamics of sheared convective boundary layer entrainment. Part I: methodological background and large-eddy simulations. J Atmos Sci 63:1151–1178
3. Conzemius RJ, Fedorovich E (2006) Dynamics of sheared convective boundary layer entrainment. Part II: evaluation of bulk model predictions of entrainment flux. J Atmos Sci 63:1179–1199
4. Conzemius RJ, Fedorovich E (2007) A case study of convective boundary layer development during IHOP: numerical simulations compared to observations. Mon Wea Rev, to appear
5. Deardorff JW (1980) Stratocumulus-capped mixed layers derived from a three-dimensional model. Bound-Layer Meteor 18:495–527
6. Fedorovich E, Conzemius RJ, Mironov D (2004) Convective entrainment into a shear-free, linearly stratified atmosphere: bulk models reevaluated through large eddy simulations. J Atmos Sci 61:281–295
7. Fedorovich E, Nieuwstadt FTM, Kaiser R (2001) Numerical and laboratory study of a horizontally evolving convective boundary layer. Part I: transition regimes and development of the mixed layer. J Atmos Sci 58:70–86
8. Khanna S, Brasseur JG (1998) Three-dimensional buoyancy and shear-induced local structure of the atmospheric boundary layer. J Atmos Sci 55:710–743
9. Moeng CH, Dudhia J, Klemp J, Sullivan PP (2007) Examining two-way grid nesting for large eddy simulation of the PBL using the WRF model. Mon Wea Rev 135:2295–2311
10. Moeng CH, Sullivan PP (1994) A comparison of shear and buoyancy-driven planetary boundary layer flows. J Atmos Sci 51:999–1022
11. Nieuwstadt FTM (1990) Direct and large-eddy simulation of free convection. In: Proc 9th Internat Heat Transfer Conference 1:37–47. Amer Soc Mech Engrg, New York, Jerusalem, Israel
12. Pino D, Arellano J, Duynkerke PG (2003) The contribution of shear to the evolution of a convective boundary layer. J Atmos Sci 60:1913–1926
13. Scipión D, Chilson PB, Fedorovich E, Palmer RD (2007) A radar simulator based on large eddy simulation for studies of the daytime convective boundary layer. J Atmos Oceanic Technol, submitted
14. Sorbjan Z (2004) Large-eddy simulations of the baroclinic mixed layer. Bound-Layer Meteor 112:57–80
15. Sullivan PP, Moeng CH, Stevens B, Lenschow DH, Mayor SD (1998) Structure of the entrainment zone capping the convective atmospheric boundary layer. J Atmos Sci 55:3042–3064